International Journal of Advanced Engineering and Technology Research
ISSN: 3106-8677 (Print), ISSN: 3106-8685 (Online) | Vol. 1, No. 2, 2026

Temperature Field Prediction of Polypropylene Yarns in Fabric-Based Evaporators for Solar Seawater Desalination

Hao Wang [1], Jiahui Song [2], Anqi Lin [3], Haoyu Zhou [3], Yongfeng Guo [1] *

[1] School of Computer Science and Technology, Tiangong University, Tianjin, China

[2] School of Advanced Interdisciplinary Studies, Tiangong University, Tianjin, China

[3] School of Textile Science and Engineering, Tiangong University, Tianjin, China

[*] **Corresponding author**: (Email: sdjnwsgyf@163.com)

Abstract: To accurately predict the temperature field in the horizontal segment of polypropylene yarns for solar-driven seawater desalination fabrics, this study performed experimental tests and modeling analysis. 900D polypropylene yarns were prepared to build a temperature test system, with data measured by an infrared thermal imager. A multiphysics coupling temperature field prediction model was developed as the core work: the unsteady conduction-convection coupled heat transfer control equation of yarns was derived, the 1D Richards equation was adopted for capillary liquid transport characterization, and the interfacial evaporation rate quantification model was coupled. The governing equations were iteratively solved after steady-state transformation, spatial discretization and second-order central difference discretization. Experimental verification showed high consistency between model predictions and measured data (RMSE= 0.92, average relative error=2.01%), which accurately reveals the gradual rise of yarn temperature from the water supply end to the evaporation far end. The study also analyzed model limitations such as idealized assumptions and parameter source issues, and proposed optimization directions including multi-dimensional modeling and experimental measurement of key parameters. It clarifies the essence of heat transfer before constructing the temperature field model, accurately reveals the heat and mass transfer correlation at the yarn scale, and provides a theoretical basis for the performance improvement of fabric-based evaporators.

Keywords: Temperature field prediction, Numerical simulation, Heat and mass transfer in porous media.

1. Introduction

With the worsening global water shortage, solar-driven seawater desalination technology has emerged as an effective remedy for the freshwater crisis owing to its clean and sustainable merits [1]. Among various solar evaporators, fabric-based interfacial evaporation systems have become a research hotspot for their strong capillary water supply capacity, flexible structure and low cost [2]. Composed of hydrophobic floating substrates and hydrophilic evaporation fabrics, these systems deliver water to the evaporation interface by capillary action and realize continuous evaporation via solar radiation heating. As the core unit for water transport and evaporation in the system, yarns exert a pivotal effect on the overall evaporation and energy utilization efficiency through their internal heat and mass transfer laws.

In recent years, numerous studies on fabric-based seawater evaporators have been conducted, and a series of high-efficiency evaporators have been developed, demonstrating the great flexibility of fabric-based systems in structural design and functional integration. Peng et al. designed a nature-inspired upward hanging 3D spacer fabric evaporator with a reverse water supply mode, achieving an evaporation rate of 2.81 $kg \cdot m^{-2} \cdot h^{-1}$ at a 52° tilt angle with a heat loss of only 0.366 W, which provides a new idea for zero-liquid-discharge desalination [3]. Kong et al. constructed a fabric evaporator based on ionic covalent organic frameworks; the material's full-spectrum absorption capacity and excellent hydrophilicity significantly improved evaporation performance, with an ion removal rate of 99.7% meeting the WHO drinking water standards [4]. Xia et al. developed an all-cellulose-based wicking fabric evaporator that reduces water evaporation enthalpy via its unique hydrophilic network structure and exhibits outstanding anti-salt crystallization performance, with a daily outdoor freshwater collection of up to 8.39 $kg \cdot m^{-2}$ [5]. Li et al. designed a multi-functional layer fabric evaporator inspired by towel structures; the surface loop structure increased solar absorption to 96.2%, and the bottom hydrophilic layers enabled efficient water storage and transport, leading to a high evaporation rate of 3.72 $kg \cdot m^{-2} \cdot h^{-1}$ under the synergy of sunlight and wind [6]. Li Yaping et al. designed an integrated fabric evaporator composed of polypropylene yarns and polyethylene foam, achieving an evaporation rate of 1.408 $kg \cdot m^{-2} \cdot h^{-1}$ under 1 sun irradiation with excellent anti-salt performance [7].

Most of the above studies focus on improving the macroscopic evaporation performance and realizing anti-salt functions of fabric-based evaporators via material modification and structural design, but in-depth investigations on the multiphysics coupling mechanism at the yarn scale—especially the accurate modeling and quantitative analysis of temperature field distribution in the horizontal yarn segment—are still lacking. In the field of heat and mass transfer in porous media, relevant mechanistic studies have been carried out: Li et al. established a 3D multiphysics model for columnar evaporators to reveal the formation and evolution mechanism of mixed temperature gradients [8]; Fillet et al. constructed a 2D axisymmetric heat and mass transfer model based on bio-based foam materials to analyze the effects of environmental conditions and structural design on evaporation performance [9]; Fan et al. proposed a non-uniform capillary model to explore the influence of pore structure on liquid transport in fiber assemblies [10]. These studies provide an important theoretical basis for heat and mass transfer in porous media, but their research objects are mostly bulk materials or simplified capillary models. They neither focus on the flexible polypropylene yarns of fabric-based evaporators nor the inhomogeneous temperature field distribution caused by saturation gradients in the horizontal segment under end water supply, and there is a lack of temperature field prediction models suitable for such yarns.

In practical fabric-based solar seawater desalination systems, the horizontal segment of polypropylene yarns forms an axial saturation gradient under end water supply, which further leads to spatial inhomogeneity of the temperature field. This distribution law directly reflects the intrinsic mechanism of hydrothermal coupling transport and is the key to efficient and stable system evaporation. Therefore, establishing a mathematical model capable of accurately predicting the temperature field in the horizontal segment of polypropylene yarns has important theoretical and engineering significance for revealing the hydrothermal coupling mechanism of fabric-based evaporators, guiding yarn structural optimization and improving overall system performance.

Based on this, this study takes the 900D hydrophilic polypropylene yarn wrapped on a polyethylene foam substrate as the core research object, and conducts experimental and modeling research on the temperature field distribution in its horizontal segment. A temperature field test system was built to obtain measured data of the yarn's horizontal segment via an infrared thermal imager. A one-dimensional steady-state multiphysics coupling model for temperature field prediction was constructed, which comprehensively considers various energy transport mechanisms including capillary-driven liquid water flow, unsteady coupled conduction-convection heat transfer, solar radiation absorption, latent heat loss of evaporation, and convective and radiative heat transfer. The internal heat transfer control equation of the yarn was derived; the one-dimensional Richards equation was adopted to characterize capillary liquid transport, and the interfacial evaporation rate quantification model was coupled. Discrete iterative solution of the control equations was realized through steady-state transformation, spatial discretization and the second-order central difference scheme. The model accuracy was verified by comparing numerical simulation with measured data, and the intrinsic correlation between the saturation gradient and temperature field distribution in the yarn's horizontal segment was revealed. Meanwhile, the model limitations were analyzed and future optimization directions were proposed, providing theoretical modeling support for the yarn structural design and performance prediction of fabric-based solar seawater desalination systems.

2. Experimental Methods and Materials

2.1. Experimental Materials

Black polypropylene filament yarn was procured from Changzhou Guoxing Special Chemical Fiber Co., Ltd.; polyethylene foam substrate was sourced from Kunshan Hongyixuan E-commerce Co., Ltd.; customized water tanks filled with distilled water were utilized to simulate an aqueous environment; temperature fields were measured using a VarioCAM® HD high-resolution infrared thermal imager from InfraTec (Germany); ambient temperature and humidity data were recorded with a WS101 thermohygrometer manufactured by Tianjin Kehui Instrument Factory; solar irradiance was quantified using a CEL-NP-2000 high-intensity optical power meter supplied by Beijing Zhongjiaojinyuan Technology Co., Ltd. All instruments were operated within their valid calibration periods.

2.2. Preparation of Experimental Materials

The research object of this experiment was 900D strand made by combining multiple polypropylene long filament yarns. The preparation method is as follows:

Table 1. Yarn Parameter Table

Sample	Low twist factor (150)
	Twist of yarn (twist/10cm)
75D/72F	15

Using the DSTw-01 type twisting machine, 12 strands of 75D/72F polypropylene filament yarns were twisted together to produce a 900D yarn.

2.3. Temperature Field Distribution Test

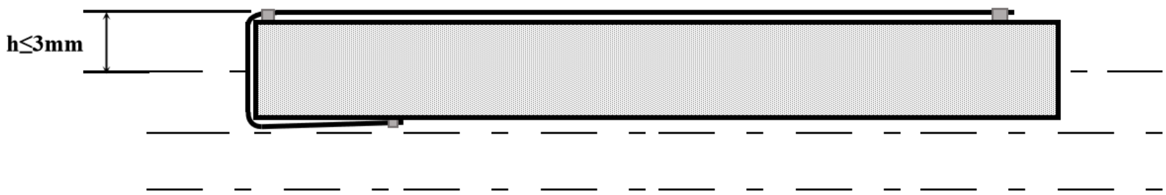

Figure 1. Experimental Setup Diagram

To facilitate independent research, first, customized plastic buckles are fixed at both ends of the foam block along its length to secure the two ends of the yarn, thereby supporting and thermally isolating the yarn. Then, the entire system was placed in a water tank filled with distilled water, and weights were placed above the foam block to control the float height, ensuring that the upper surface of the foam block was no more than 3 mm higher than the water surface, so that the side yarns could be basically immersed in water, which was conducive to the subsequent temperature field test in the horizontal section. The system was placed in a stable atmospheric environment, and the environmental temperature and humidity as well as the solar radiation power were recorded. After the capillary process was completed, the yarn was photographed from the front using the VarioCAM® HD infrared thermal imager. The measurement range, spatial resolution and sampling frequency of this thermal imager are all suitable for the expected environmental temperature changes. For each condition, the thermal image sequence was continuously recorded for no less than 30 minutes, and the temperature data at each position of the yarn was extracted using the IRBIS 3 plus software for visualization and temperature gradient analysis.

3. Establishment of the Temperature Field Prediction Model

In the practical application of solar-driven seawater desalination fabrics, the system couples multiple physical processes: liquid migration in yarns, energy transmission, and water vaporization. Yarns' microcapillary structures deliver seawater continuously to the evaporation interface via capillary effect for liquid water mass transfer. As the main energy source, solar radiation warms foam-attached yarns to drive evaporation. The system's end-fed water supply creates a saturation gradient along yarn water transport, causing spatially non-uniform temperature field, showing distinct multiphysical coupling and spatial gradient behaviors.

To quantify and predict these complex processes, this study focuses on investigating and predicting the temperature field distribution in the horizontal segment.

3.1. Derivation of Heat Transfer Model Inside Yarn

The yarn is a porous medium characterized by the coexistence of solid, liquid, and gas phases, wherein unsteady fluid flow and heat exchange occur. To accurately quantify the energy transport in this process, this study starts from Fourier's law of heat conduction and initially considers the coupled effects of fluid convective heat transfer and effective thermal conduction in the porous medium, focusing on the spatiotemporal evolution of the temperature field. However, given that the capillary-driven liquid flow velocity is extremely low (typically on the order of mm/h), the sensible heat convection is negligible compared to latent heat of phase change and thermal conduction. Consequently, the control equation simplifies to the form of unsteady heat conduction with an effective thermal conductivity, which is expressed as follows:

$$\rho c \frac{\partial T}{\partial t} = \frac{\partial}{\partial z}\left[k_{eff}\frac{\partial T}{\partial z}\right] + q \tag{1}$$

Where, ρ is the overall density of the yarn (kg/m^3); c is the overall isobaric specific heat capacity of the yarn (J/(kg·K)); T is the yarn temperature (K); k_{eff} is the effective thermal conductivity of the yarn (W/(m·K)); t and z are the time (s) and axial spatial variable (m), respectively. Here, q represents the net energy flux per unit volume of the yarn at the open evaporation interface, which balances the solar energy input against major energy losses and will be further elaborated in the following context.

The non-uniform distribution of water and air phases inside the yarn poses great challenges to establishing a realistic and reliable heat transfer model. This study simplifies the actual heat transfer problem in porous media into an equivalent solid heat transfer problem. Based on the effective medium theory, the effective thermophysical properties of the three-phase system are obtained, which supports the formulation and solution of the governing equations.

The density and isobaric specific heat capacity of the mixture fluid are obtained by weighting the intrinsic parameters of water and air with saturation. The saturation S_r characterizes the occupancy of water in the yarn pores, and the calculation formulas are as follows:

$$(c\rho)_f = S_r\rho_w c_w + (1-S_r)\rho_a c_a \tag{2}$$

$$\rho c = (1-\phi)(\rho c)_s + \phi(\rho c)_f$$

Where, ρ_w and ρ_a are the densities of water and air, with the values of 997 kg/m^3 and 1.164 kg/m^3 in this study, respectively; c_w and c_a are the isobaric specific heat capacities of water and air, with the values of 4187.6 J/(kg·K) and 1013 J/(kg·K) in this study, respectively. ρc is the volumetric heat capacity of the three-phase mixture, which is obtained by weighting the volumetric heat capacity of the solid skeleton and that of the mixed fluid according to their volume fractions.

The effective thermal conductivity k_{eff} is calculated by weighting the thermal conductivities of the solid, liquid and gas phases according to the volume fraction. The porosity ϕ characterizes the volume ratio of pores inside the yarn, with a value of 0.73 in this study, and the calculation formulas are as follows:

$$k_{eff} = (1-\phi)k_s + \phi[S_r k_w + (1-S_r)k_a] \tag{3}$$

Where, k_s is the thermal conductivity of the yarn solid matrix; k_w and k_a are the thermal conductivities of water and air, with the values of 0.606 W/(m·K) and 0.026 W/(m·K) in this study, respectively, and the thermal conductivity k_s of the solid matrix is 0.17 W/(m·K).

At the open evaporation interface, the net energy flux q balances solar input against three loss pathways:

$$q = q_s - q_c - q_r - q_l \tag{4}$$

Each flux term (normalized to unit yarn volume) is defined as:

$q_s = I\alpha A_s/V_y$: Solar radiation absorption flux (I: solar irradiance, α : absorptivity, A_s : illuminated area, V_y : yarn volume);

$q_c = h(T - T_0)A_h/V_y$: Convective heat loss flux (h : convective coefficient, T_0 : ambient temperature, A_h : convective area);

$q_r = \dfrac{\varepsilon\sigma(T_a^4 - T^4)A_r}{V_y}$: Net radiative heat loss flux (ε : emissivity, σ : Stefan-Boltzmann constant, A_r : radiative area);

$q_l = \dot{m}\,\Delta H_v \dfrac{A_e}{V_y}$: Latent heat loss flux ($\dot{m}$: represents the evaporation rate per unit area, and it is converted to a volumetric heat sink by multiplying the specific evaporation area A_e/V_y, ΔH_v : latent heat of vaporization).

Substituting q into Eq. (1) yields the closed heat transfer equation, which fully couples liquid water transport and interfacial evaporation, forming the mathematical basis for subsequent numerical solution of the yarn temperature field.

3.2. Establishment of Liquid Water Transport Model Inside Yarn

Liquid water transport in the unsaturated yarn is dominated by capillary forces, which can be precisely characterized by the one-dimensional Richards equation:

$$\frac{\partial(\phi S)}{\partial t} = \frac{\partial}{\partial z}\left(D(S)\frac{\partial S}{\partial z}\right) - E_s \quad (5)$$

$$E_s = \frac{\dot{m}}{\rho_w} \cdot \frac{A_e}{V_y}$$

Where ϕ is the effective porosity of the yarn, fixed at 0.73; S denotes the liquid water saturation, representing the volume fraction of liquid water in pore spaces. E_s is the sink term of volumetric evaporation rate per unit pore. ρ_w represents the density of liquid water.

The water diffusion coefficient $D(S)$ exhibits a strong saturation-dependent behavior [11], modeled using a modified van Genuchten power-law relation—an alternative empirical framework for unsaturated flow in porous media:

$$D(S) = D_{\max} \cdot S^n \cdot \left[1 - \left(1 - S^{1/m}\right)^m\right]^2 \quad (6)$$

Here, D_{max} is the maximum diffusion coefficient under fully saturated conditions, while n and m are fitting parameters related to the pore size distribution (set to $n=3$ and $m=0.5$ in this work, consistent with the original pore structure characteristics).

D_{max} is derived from the combination of the Hagen-Poiseuille equation for capillary flow and Darcy's law, yielding:

$$D_{\max} = \frac{\gamma r \cos\theta}{2\eta m} \quad (7)$$

Where γ is the surface tension of water (0.0759 N/m), θ is the contact angle between water and the yarn's solid capillary walls (66°), η is the dynamic viscosity of water (0.0008545 Pa·s), r is the characteristic radius of the yarn's micropores, and m is the structural fitting parameter defined above.

3.3. Quantification of Evaporation Rate at Open Evaporation Interface

The evaporator is in an open atmospheric environment, and interfacial evaporation causes energy dissipation and mass loss of the yarn, which is a key factor affecting the temperature field distribution. Therefore, it is necessary to first quantitatively calculate the local evaporation rate of the yarn. Based on the basic principles of mass transfer and combined with the characteristics of gas-phase mass transfer and saturated vapor pressure, this study establishes a calculation model for the local evaporation rate of the yarn, and its core expression is as follows:

$$\dot{m} = \beta_m \cdot \frac{M_{H_2O}}{R} \cdot \left(\frac{P_{sat}(T)}{T} - \frac{RH \cdot P_{sat}(T_0)}{T_0}\right) \quad (8)$$

Where, β_m is the convective mass transfer coefficient between the yarn and the environment (m/s); M_{H_2O} is the molar mass of water molecules (kg/mol); R is the ideal gas constant (J/(mol·K)); RH is the relative humidity of the ambient air; T and T_0 are the local evaporation temperature of the yarn and the ambient temperature (K), respectively; $P_{sat}(T)$ and $P_{sat}(T_0)$ are the saturated vapor pressures of water at temperatures T and T_0 (Pa), respectively.

Saturated vapor pressure is a function of temperature. In this study, the Clapeyron-Clausius equation is used to calculate the saturated vapor pressure at different temperatures. This equation can accurately reflect the thermodynamic relationship between the saturated vapor pressure of pure substances and temperature. Combined with the phase change characteristics of water, its simplified form is as follows:

$$\ln\frac{P_{sat}(T)}{P_0} = \frac{\Delta H_v}{R_w} \cdot \left(\frac{1}{T_b} - \frac{1}{T}\right) \quad (9)$$

Where, P_0 is the standard atmospheric pressure (Pa); ΔH_v is the latent heat of vaporization of water (J/kg); T_b is the boiling point temperature of water under standard atmospheric pressure (K). The rapid calculation of saturated vapor pressure at any temperature can be realized through this equation, which provides a basis for the quantification of evaporation rate; R_w is the specific gas constant of water vapor, 461J/(kg·K).

4. Numerical Calculation of the Temperature Field in the Horizontal Segment

4.1. Steady-State Analysis

Analysis indicates that, although the system undergoes a rapid dynamic transition process, it eventually reaches a steady state. For the steady state, it satisfies:

$$\frac{\partial S}{\partial t} = 0, \quad \frac{\partial T}{\partial t} = 0 \quad (10)$$

Therefore, the model is transformed from a system of binary partial differential equations (PDEs) into a system of ordinary differential equations (ODEs), and the mass conservation equation becomes:

$$\frac{d}{dz}\left[D(S)\frac{dS}{dz}\right] = E_s \quad (11)$$

Due to the extremely slow velocity of capillary-driven liquid water flow, the sensible heat convection transport is negligible compared to the latent heat of phase change and thermal conduction. So the energy conservation equation becomes:

$$\frac{d}{dz}\left[k_{eff}\frac{dT}{dz}\right] = -q \quad (12)$$

4.2. Spatial Discretization and Difference Scheme

Since the model we established is a one-dimensional model along the axial direction (z-axis) of the yarn, during the solution process, we divide the computational domain

$z \in [0, L]$ into N equal control volumes based on the concept of control volumes. The nodes are located at the centers of these control volumes, and their positions are expressed as:

$$z_i = i\Delta z \ , \quad i = 0, 1, \ldots, N \tag{13}$$

Here, $\Delta z = L/N$. For the system investigated in this study, L represents the horizontal length of the yarn. To ensure computational accuracy and efficiency, N was selected as 200 after grid independence verification.

Under steady-state conditions, time derivatives vanish, simplifying governing equations to ODEs. A second-order central difference scheme discretizes spatial derivatives. Iterative expressions for saturation and temperature are derived: saturation involves evaporation rate and arithmetically averaged interfacial diffusion coefficients; temperature uses arithmetically averaged effective thermal conductivity and an internal heat source (solar absorption, convection, radiation, latent heat). Iterative calculation yields the steady-state temperature field.

5. Results and Analysis

5.1. Results Presentation

Substituting the relevant parameters of the yarn and the environment (solar irradiation power: 1004.3 W/m^2, temperature: 44°C, humidity: 50%), the steady-state solver was invoked to compute the temperature field distribution T(z) along the axial direction (z-direction) of the yarn, as shown in Figure 2.

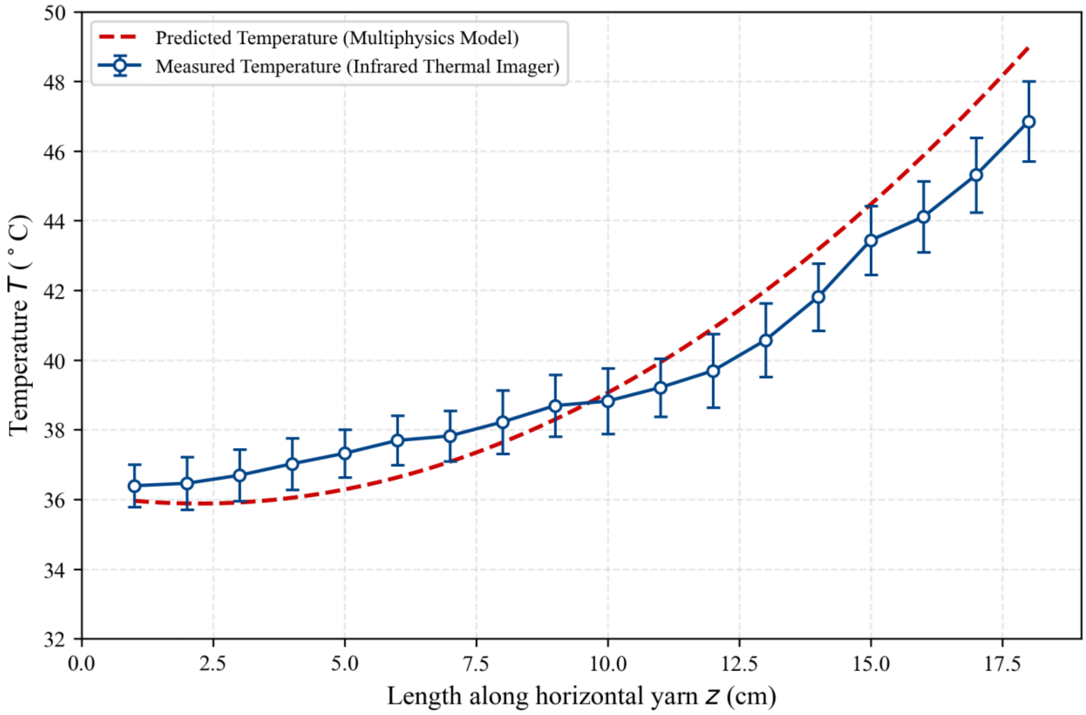

Figure 2. Predicted and measured temperature field distribution curves

As shown in the figure, the temperature of all yarns exhibits a gradually increasing trend from the water supply end to the far end of the evaporation section. This phenomenon can be attributed to the spatial distribution of saturation within the yarn: near the water supply end, capillary action continuously replenishes moisture, resulting in higher saturation and water content within the yarn. Consequently, the temperature increases slowly, leading to lower temperatures in this region and a slow evaporation process. As the axial distance increases, the water supply gradually diminishes, saturation decreases, and the water content reduces. Meanwhile, continuous solar radiation input causes heat to accumulate within the yarn, thereby progressively increasing the temperature. A comparison between the experimental data and simulation results demonstrates high consistency. The root mean square error (RMSE) of the model predictions was 0.92, and the average relative error was 2.01%, further validating the accuracy and generalizability of the multiphysics coupling model established in this study for predicting the temperature field of the yarn. These results also indicate that the model effectively captures the coupling mechanism between water transport and heat transfer.

5.2. Limitations Analysis

Although the numerical model constructed in this study can effectively predict the temperature field distribution in the horizontal segment of the yarn, the following limitations remain:

Idealized Model Assumptions: The model simplifies the yarn as a homogeneous one-dimensional porous medium, neglecting the anisotropy caused by the actual twisted structure.

Constraints in the Source of Key Parameters: Parameters involved in the model, such as pore radius, contact angle, and diffusion coefficient, rely heavily on empirical formulas or reference values from the literature, which may increase the error in simulation results.

Fluctuations in Experimental Validation Conditions: Environmental factors (e.g., wind speed, humidity) during the experiment were difficult to maintain perfectly constant, which affected the accuracy of model validation to some extent.

6. Conclusions and Prospects

In this study, a one-dimensional steady-state numerical model based on multiphysics coupling was developed to investigate the temperature field distribution in the horizontal segment of polypropylene yarns used in solar-driven seawater desalination fabrics. The model comprehensively considered various energy transport mechanisms, including capillary-driven liquid flow, unsteady heat conduction, latent heat of evaporation, solar radiation absorption, convective heat transfer, and radiative heat transfer. The governing equations were discretized and solved using the finite difference method. Comparison between experimental and simulation results indicated that the temperature field of the yarn exhibited a gradually increasing trend from the water supply end to the far end of the evaporation section. The model predictions were in good agreement with the measured data, with a root mean square error (RMSE) of 0.92 and an average relative error of 2.01%. These results validated the accuracy of the proposed model and demonstrated its capability to effectively capture the coupling mechanism between water transport and heat transfer.

Based on the findings of this study, future work can be explored in the following aspects: introducing two-dimensional or three-dimensional models to account for the influence of the yarn's micro-pore structure; conducting experimental measurements of key material parameters to reduce uncertainty in model inputs; extending the model to unsteady-state conditions to investigate response characteristics under dynamic environments; and incorporating multiscale coupling analysis to achieve system-level performance predictions. These efforts will provide a more solid theoretical foundation for the optimal design and practical application of solar-driven seawater desalination fabrics.

Acknowledgment

This invention was supported by the National College Students' Innovation and Entrepreneurship Training Program of Tiangong University (Project No.: 202510058029).

References

[1] Liu Z, Xingxing Z, Zhang W, et al.Recent Advances in carbon-based photothermal materials for solar interface evaporation-driven seawater desalination [J]. Chemical Engineering Journal, 2025, 525170563-170563. DOI:10.1016/J.CEJ.2025.170563.

[2] Liu F, Liu X, Liu Q, et al. Fabric-based all-in-one evaporator for high-performance solar desalination: An analytic hierarchy process evaluation [J]. Applied Thermal Engineering, 2026, 290(P1): 129998-129998. DOI:10.1016/J.APPLTHERMALENG.2026.129998.

[3] Peng Y, Shao Y, Zheng L, et al. Nature-Inspired Upward Hanging Evaporator with Photothermal 3D Spacer Fabric for Zero-Liquid-Discharge Desalination [J]. Nano-Micro Letters, 2025, 18(1):22-22. DOI:10.1007/S40820-025-01868-0.

[4] Kong W, Ma Y, Huang H, et al. Fiber fabric evaporators based on ionic COFs for solar interfacial evaporation and seawater desalination [J]. Chemical Engineering Journal, 2025, 520166125-166125. DOI:10.1016/J.CEJ.2025.166125.

[5] Xia F, Tian Y, Zhang X, et al. Architecting of All-Cellulose-Based Wicking Fabric for a Large-Scale, Low-Cost, and Highly Efficient Solar Desalination Evaporator [J]. ACS nano, 2025, 19(9):8608-8620. DOI:10.1021/ACSNANO.4C14352.

[6] LiJ, GeC, HeJ, et al. Towel-Inspired Fabric-Based Evaporator for Highly Efficient Water-Evaporation Desalination [J]. Advanced Materials Technologies, 2023, 9(2): DOI:10.1002/ADMT.202301368.

[7] YAPING LI. Scalable Fabric-Based Solar Steam Generator [J]. Advanced Functional Materials, 2024, 34 22. DOI:10.1002/adfm.202312613.

[8] Li Y, Liu X, Hong W, et al. Formation, evolution, and enhancement mechanisms of mixed temperature gradient during interfacial solar vapor generation [J]. International Journal of Heat and Mass Transfer, 2023. DOI:10.1016/j.ijheatmasstransfer.2023.124082.

[9] Fillet R, Nicolas V, Fierro V, et al. Modelling heat and mass transfer in solar evaporation systems [J]. International Journal of Heat and Mass Transfer, 2021, 181:121852-1 – 121852-14. DOI:10.1016/j.ijheatmasstransfer.2021.121852.

[10] Jie F, Cai-Xia L, Yuan-Yuan Q, et al. Liquid transport in non-uniform capillary fibrous media [J]. Textile Research Journal, 2018:004051751877924. DOI:10.1177/0040517518779248.

[11] Wang Y, Sun H, Ni T, et al. A hybrid fractional-derivative and peridynamic model for water transport in unsaturated porous media [J]. Fractals, 2023, 31(7). DOI:10.1142/S0218348X23500809.